

NAG 1-8

DAA/LANGLEY

1N-02

76872-CR

P.35

TRANSONIC FLOW SOLUTIONS USING A COMPOSITE
VELOCITY PROCEDURE FOR POTENTIAL, EULER AND RNS EQUATIONS

R. E. Gordnier and S. G. Rubin

Department of Aerospace Engineering and Engineering Mechanics
University of Cincinnati
Cincinnati, Ohio 45221

Abstract

Solutions for transonic viscous and inviscid flows using a composite velocity procedure are presented. The velocity components of the compressible flow equations are written in terms of a multiplicative composite consisting of a viscous or rotational velocity and an inviscid, irrotational, potential-like function. This provides for an efficient solution procedure that is locally representative of both asymptotic inviscid and boundary layer theories. A modified conservative form of the axial momentum equation that is required to obtain rotational solutions in the inviscid region is presented and a combined conservation/non-conservation form is applied for evaluation of the reduced Navier-Stokes(RNS), Euler and potential equations. A variety of results are presented and the effects of the approximations on entropy production, shock capturing and viscous interaction are discussed.

1. Introduction

The composite velocity formulation developed by Rubin and Khosla[1] is a boundary layer like relaxation procedure based on a multiplicative composite velocity. For the Navier-Stokes or reduced Navier-Stokes (RNS) equations it provides a technique that is consistent with both

N87-25995

(NASA-CR-180435) TRANSONIC FLOW SOLUTIONS
USING A COMPOSITE VELOCITY PROCEDURE FOR
POTENTIAL, EULER AND RNS EQUATIONS
(Cincinnati Univ.) 35 p Avail: NTIS HC
AC3/MF A01 CSCL 01A G3/02

Unclass
0076872

asymptotic inviscid theory and boundary layer theory. The composite velocity formulation is directly applicable to incompressible, subsonic, transonic and supersonic flows. The solution procedure is identical in all cases. Supersonic regions are modelled with the Enquist-Osher approximation.

In this formulation a multiplicative composite for the velocities is defined, see reference (1). A viscous or rotational velocity (U) and a pseudo-potential or irrotational velocity (ϕ_x, ϕ_y) are specified. This allows for the application of procedures developed for the transonic potential equation to be adapted to a composite velocity Euler and RNS formulation. Finally, the composite splitting provides for greater flexibility, since the viscous and inviscid portions of the velocity fields are easily identified.

The composite velocity formulation has previously been used to determine incompressible [2], subsonic and transonic [3-4] flows for boattail geometries. Both laminar and turbulent flows were considered. In these studies a coupled ($U-\phi$) strongly implicit procedure [5] was used to solve the full Navier-Stokes equations. In the present study application of the composite velocity technique for both viscous and inviscid transonic flows are presented. For viscous flows a reduced form of the compressible Navier-Stokes equations, in which the viscous terms in the normal momentum equation and the streamwise diffusion terms in the axial momentum equation are neglected, is considered. The continuity and streamwise momentum equations are solved using a coupled line relaxation procedure allowing for interaction between the boundary layer and the outer inviscid flow. The Enquist-Osher flux biasing scheme for the transonic potential equation is incorporated into the

solution procedure. Finally, a Cebeci-Smith two layer model [6] is used for turbulence closure. This model is acceptable for the attached or mildly separated wall layers considered herein.

Verification of solution accuracy, in the outer inviscid region of a viscous interacting flow field, has been considered by solving the inviscid Euler equations. The composite velocity equations are still specified, but with slip boundary conditions and infinite Reynolds number (Re). Both irrotational, isentropic (potential) solutions and rotational, nonisentropic (Euler) solutions may be calculated with the $Re = \infty$ and slip boundary conditions. A conservation form of the composite velocity equations is required for transonic Euler solutions; a non-conservation form generates the full potential solution. The conservation form for the Euler equations is shown to generate a correct entropy rise at the shock wave, while the non-conservation form does not generate spurious entropy in non shock regions.

2. Governing Equations

The Navier-Stokes equations for steady, compressible flow of a perfect gas are given in general, orthogonal, curvilinear coordinates as follows:

Continuity

$$(\rho h_2 h_3 u)_\xi + (\rho h_1 h_3 v)_\eta = 0 \quad (1)$$

ξ -Momentum

$$\begin{aligned} \frac{1}{h_1} \rho u u_\xi + \frac{1}{h_2} \rho v u_\eta + \frac{1}{h_1 h_2} \rho u v h_{1\eta} - \frac{1}{h_1 h_2} \rho v^2 h_{2\xi} = - \frac{1}{h_1} p_\xi + \\ \frac{1}{D} \left[\frac{\partial}{\partial \xi} (h_2 h_3 \tau_{11}) + \frac{\partial}{\partial \eta} (h_1 h_3 \tau_{12}) \right] + \tau_{12} \frac{h_{1\eta}}{h_1 h_2} - \tau_{22} \frac{h_{2\xi}}{h_1 h_2} - \tau_{33} \frac{h_{3\xi}}{h_1 h_3} \end{aligned} \quad (2)$$

η -Momentum

$$-\frac{1}{h_1} \rho u v_{\xi} - \frac{1}{h_2} \rho v v_{\eta} - \frac{1}{h_1 h_2} \rho u v h_{2\xi} + \frac{1}{h_1 h_2} \rho u^2 h_{1\eta} = \frac{1}{h_2} p_{\eta} \quad (3)$$

$$\frac{1}{D} \left[\frac{\partial}{\partial \xi} (h_2 h_3 \tau_{12}) + \frac{\partial}{\partial \eta} (h_1 h_3 \tau_{22}) \right] = \tau_{12} \frac{h_{2\xi}}{h_1 h_2} + \tau_{11} \frac{h_{1\eta}}{h_1 h_2} + \tau_{33} \frac{h_{3\eta}}{h_2 h_3}$$

Energy

$$\frac{1}{h_1} \rho u H_{\xi} + \frac{1}{h_2} \rho v H_{\eta} = \frac{1}{D} \left[\frac{\partial}{\partial \xi} (h_2 h_3 q_1) + \frac{\partial}{\partial \eta} (h_3 h_1 q_2) \right] + \phi + \psi \quad (4)$$

where ϕ and ψ are the dissipation and viscous work terms, respectively and

$$\tau_{11} = 2\mu \left[\frac{1}{h_1} u_{\xi} + \frac{v}{h_1 h_2} h_{1\eta} \right] - \frac{2}{3} \frac{\mu}{D} [(h_2 h_3 u)_{\xi} + (h_3 h_1 v)_{\eta}]$$

$$\tau_{22} = 2\mu \left[\frac{1}{h_1} v_{\xi} + \frac{u}{h_1 h_2} h_{1\xi} \right] - \frac{2}{3} \frac{\mu}{D} [(h_2 h_3 u)_{\xi} + (h_3 h_1 v)_{\eta}]$$

$$\tau_{33} = 2\mu \left[\frac{u}{h_3 h_1} h_{3\eta} + \frac{v}{h_2 h_3} h_{3\xi} \right] - \frac{2}{3} \frac{\mu}{D} [(h_2 h_3 u)_{\xi} + (h_3 h_1 v)_{\eta}]$$

$$\tau_{21} = \tau_{12} = \mu \left[\frac{h_2}{h_1} \left(\frac{v}{h_2} \right)_{\xi} + \frac{h_1}{h_2} \left(\frac{u}{h_1} \right)_{\eta} \right]$$

$$D = h_1 h_2 h_3$$

$$q_1 = \frac{1}{h_1} k \frac{\partial T}{\partial \xi}; \quad q_2 = \frac{1}{h_2} k \frac{\partial T}{\partial \eta}; \quad \mu, k \propto T$$

In these equations, ξ and u are the coordinate and velocity measured along the body surface; η and v are the coordinate and velocity normal to the body surface; ρ is the density, p the pressure, T the temperature, and H the total enthalpy. The terms $h_1(\xi, \eta)$, $h_2(\xi, \eta)$, and h_3 are the metrics for the curvilinear coordinate system. Two additional state equations are required to complete the governing set of equations. These are

$$p = \frac{\rho T}{\gamma M_\infty^2} \quad (5)$$

and

$$\frac{p}{\rho} = \frac{1}{\gamma M_\infty^2} e^{\gamma(\gamma-1)M_\infty^2(S-1)} \quad (6)$$

where S is entropy.

The composite velocity formulation procedure developed by Rubin and Khosla[1] is employed to represent the velocity fields. In the spirit of matched asymptotic expansions, the velocities are re-written as

$$u = \frac{(U+1)}{h_1}(1+\phi_\xi) = (U+1)u_e \quad (7a)$$

$$v = \frac{\phi_\eta}{h_2} \quad (7b)$$

The multiplicative composite that represents the axial velocity consists of two terms, an irrotational "pseudo" potential function and a viscous velocity U . Since the change in v across the boundary layer is of the order of the boundary layer thickness, the normal velocity is determined solely by the "pseudo" potential function.

By substituting equations (7 a,b) into the Navier-Stokes equations (1-3), the following system for U , ϕ , S for 2-D ($h_3=1$) conformal ($h_2=h_1$) coordinates is obtained:

Continuity

$$[\rho(U+1)(1+\phi_\xi)]_\xi + [\rho\phi_\eta]_\eta = 0 \quad (8)$$

ξ -Momentum

$$\frac{1}{D}[(\rho h_2(U^2+U)u_e^2)_\xi + (\rho h_1 U u_e v)_\eta] + \frac{\rho}{h_1} U u_e u_{e\xi} + \quad (9)$$

$$\frac{1}{D}\rho u_e v U h_{1\eta} = \frac{\rho T}{h_1} S_\xi - \frac{\rho}{h_1} G_\xi + \text{viscous terms}$$

η -Momentum

$$TS_{\eta} = G_{\eta} + U \left[\frac{\partial}{\partial \eta} \left(\frac{u_e^2}{2} \right) - \frac{(U+1)}{h_1} u_e^2 h_{1\eta} \right] + \text{viscous terms} \quad (10)$$

where

$$G = \frac{\gamma}{\gamma-1} \frac{p}{\rho} + \frac{u_e^2 + v^2}{2}$$

$$\rho = T^{\frac{1}{\gamma-1}} e^{-\frac{\gamma M_{\infty}^2 S}{e}}$$

The new variable G , that appears in these equations is similar to the total (or Bernoulli-like) pressure. G is not, however, assumed to be constant, but is calculated by the solution procedure. The entropy S is zero in the undisturbed flow.

In the viscous region, the composite velocity formulation is representative of the full or reduced form of the Navier-Stokes equations. The continuity and ξ -momentum equations determine ϕ and U and the viscous total pressure correction is determined from the η -momentum equation. In the limit as $U \rightarrow 0$ the continuity equation reduces to the full potential equation and the Bernoulli relation, $G = \text{constant}$, is recovered. Thus, equations (9) and (10) are identically satisfied and the composite velocity system has reduced to the expected representation for an inviscid, irrotational flow.

Inviscid flows are solved by dropping the viscous terms in equations (9) and (10). The interpretation of the composite velocity terms for inviscid flows varies slightly from that for viscous flows. The ϕ term still represents an irrotational "pseudo" potential function. The U term, however, is no longer associated with the viscous effects but rather it reflects with the effects of rotationality associated with the inviscid flow; viz, the vorticity $\Omega = (h_2 v)_{\xi} - (h_1 u)_{\eta} = -(U(1+\phi_{\xi}))_{\eta}$.

The composite velocity scheme is formulated to provide solutions to the full Euler equations; if the system is solved in the non-conservation form, however, the full potential solution is recovered instead; i.e., $U=0$ everywhere and neither entropy nor vorticity is generated at any point in the flow field. This includes leading and trailing edges as well as captured shock waves. In order to capture the rotational or (Euler) shock wave in transonic flows, the ξ -momentum equation must be rewritten in a quasi-conservation form. This is obtained by substituting for S and G in the right hand side of equation (9), i.e., subtract, from the right hand side, $\frac{u_e}{h_1 h_2}$ times the continuity equation. This gives the following 'conservation' form for the ξ -momentum equation:

$$\frac{1}{D} [(\rho h_2 (U^2 + 2U) u_e^2)_\xi + (\rho h_1 U u_e v)_\eta] + \frac{1}{D} \rho u_e v U h_1_\eta = \quad (11)$$

$$-\frac{1}{h_1} (P + \rho u_e^2)_\xi - \frac{1}{h_2} (\rho u_e v)_\eta + \frac{h_2}{D} \xi (\rho v^2 + \rho u_e^2) - 2.0 \frac{h_1}{D} \eta (\rho u_e v).$$

For subsonic flows ($U=0$) and a cartesian grid ($h_1=h_2=1.0$), equation (11) reduces to the familiar conservation form of the ξ -momentum equation, i.e.,

$$(P + \rho u_e^2)_\xi + (\rho u_e v)_\eta = 0 \quad (12)$$

For transonic flow the correct entropy rise at the shock wave will now be generated. Although the correct entropy rise is predicted at the shock with the system (11), spurious entropy is also generated in non-shock regions. The generation of numerical entropy is a common problem found in many Euler solvers. Large errors in entropy may be generated at leading and trailing edges[7]. These errors may even lead to

spurious unsteady or steady solutions [8]. In the present technique a simple solution to this problem is available. The nonconservative form of the axial momentum equation (9) produces no entropy, but will accurately convect entropy or vorticity that is generated elsewhere. Therefore, this form of the axial momentum equation is used everywhere except in the shock region, where equation (11) is required. This leads to a solution procedure with the desirable feature of generating the correct entropy rise at the shock wave, but not creating spurious entropy in other regions of the flow. The advantage of non-conservative equations away from shock waves and combined conservative/non-conservative systems has been discussed in several studies by other investigators[21].

3. Boundary Conditions

As a simple test case, solutions for symmetric flow over a NACA0012 airfoil are obtained. The boundary conditions for the composite velocity formulation are easily implemented. At the inflow, $\xi=\xi_0$, uniform flow is assumed; thus $U=0$, $H=H_e$, $\phi=0$, and $S=0$. The upper boundary, $\eta=\eta_m$, is assumed to be sufficiently far from the airfoil so that the flow field is undisturbed; therefore, similar boundary conditions apply. Along the body, the viscous no-slip and zero injection conditions are used; therefore, $U=0$ and $\phi_\eta=0$. Ahead of the airfoil and in the wake, the symmetry conditions $U_\eta=\phi_\eta=0$ are imposed. At the outflow, $\xi=\xi_m$, only $\phi_\xi=0$ must be prescribed. This, in effect, assumes a weak viscous/inviscid interaction.

For inviscid flows, the no slip condition no longer applies and the zero vorticity condition $U_\eta=0$ is specified along the airfoil. At the

outflow, $\xi=\xi_m$, the boundary condition $\phi=0$ is imposed. The remaining boundary conditions are unchanged.

4. Finite Differencing

The Enquist-Osher flux biasing scheme[9] for transonic flows has been adapted for differencing the continuity equation. This scheme, which has been developed for the full potential equation, produces very sharp shocks and guarantees that expansion shocks do not occur. This scheme consists of defining a modified density $\bar{\rho}$, such that

$$\bar{\rho}_{i,j} = \rho_{i,j} - \frac{\Delta x}{q_{i,j}} ((\rho q)_-_{i,j} - (\rho q)_-_{i-1,j}) \quad (13)$$

where

$$(\rho q)_- = 0.0 \quad \text{if } M \leq 1$$

$$(\rho q)_- = \rho q - \rho^* q^* \quad \text{if } M \geq 1$$

Here ρ^* and q^* are the sonic velocity and density. The modified density $\bar{\rho}$ is then used in the $[\rho(1 + \phi_\xi)]$ portion of the ξ -derivative in the continuity equation.

The $[\rho(U+1)(1+\phi_\xi)]_\xi$ derivative is approximated with a two point backward difference and the ϕ_ξ derivative is approximated with a two point forward difference. The modified density $\bar{\rho}$ is applied as discussed previously. The $[\rho\phi_\eta]_\eta$ is differenced in a similar manner, when v is less than zero. When the v velocity is greater than zero, however, this term is forward differenced and ϕ_η is approximated with a two point backward difference. Central differencing results for subsonic regions.

In the ξ -momentum equation (9), the $(\rho h_2 (U^2 + U) u_e^2)_\xi$ derivative is approximated with two or three point backward differences. For viscous flows, upwind differencing is applied in regions of reversed flow. The convective term is identically zero at the separation and reattachment points. The $(\rho h_2 U u_e v)_\eta$ and U_{e_ξ} (or $\rho_{\xi\xi}$) terms are approximated with second order accurate central differences. For the S_ξ and G_ξ terms on the right hand side, two point backward differences are applied. When the conservation form, equation (11), is used, a two point backward difference is used for $(p + \rho u_e^2)_\xi$ and central differencing is used for $(\rho u_e v)_\eta$.

Backward differencing of the ξ -derivatives provides for the proper convection of U in inviscid regions. If a value of U (i. e. vorticity) is generated, this value will be convected downstream in one global pass. Moreover, in the non-conservation form the value of the vorticity is conserved and additional numerical vorticity is not generated even at the trailing edge of an airfoil.

The discretized continuity and ξ -momentum equations are solved for U and ϕ with a coupled line relaxation procedure. The values of ρ , S , and G in the equations are given from the previous iteration. From the values of U and ϕ , the entropy variation is determined from the η -momentum equation. This equation is solved using the standard trapezoidal rule.

For the large Reynolds number moderately separated flows considered herein, a Cebeci-Smith two layer eddy viscosity model is used to close the system of governing equations. The coefficient of viscosity is given as

$$\mu = \mu_l + \mu_t \quad (14)$$

where μ_l is the laminar viscosity and μ_t is the turbulent eddy viscosity, as prescribed by the Cebeci-Smith model. Details of this closure model are found in reference 3. The onset of turbulence was specified at 5% of the chord. The actual transition location is not well known, but is approximated reasonably with the present assumption.

5. Results

Viscous and inviscid solutions for transonic flow have been obtained for the symmetric flow over a NACA0012 airfoil. A Schwartz-Christoffel mapping procedure developed by Davis [10] generates the required grid, figure 1. The flow region is defined from an upstream location of $\xi = -4.6$ to an outflow boundary $\xi = 6.89$. The airfoil is located between $\xi = 0.0$ and $\xi = 1.0$. In the tangential direction, 105 grid points are prescribed; this includes 60 points on the body, 20 points ahead of the body, and 25 points aft of the body. A uniform mesh is defined on the body and a mesh stretch factor of 1.18 is used ahead of and aft of the body. In the η direction, there are 50 grid points, so that the flow region extends from $\eta = 0.0$ to $\eta = 22.0$. For viscous flows, an initial grid spacing of $\Delta\eta = 0.0001$ is prescribed; a stretch factor of 1.25 is assumed for the remaining mesh development. For inviscid flows, the initial grid spacing in the η -direction is $\Delta\eta = 0.02$, since the boundary layer need not be resolved.

To verify that the algorithm correctly calculates the inviscid portion of the flow, a full potential solution for $M_\infty = 0.85$ is obtained. Full potential solutions are obtained directly from the set of equations (8-10) by solving the axial momentum equation in the non-conservation form given by equation (9). In this form, U and S are calculated to be

identically zero and therefore the full potential solution is recovered for ϕ . The present solution is compared with results of the GAMM workshop on transonic flows [11], figure 2. The workshop results indicate a wide variation in shock location and strength and the figure depicts only the lower and upper bounds of the workshop solutions. Comparison with other potential solutions, in the published literature and for the same case, indicate that this scatter of solutions to the full potential equation is not unusual, figure 3. The present calculation produces a very sharp shock and the shock falls within the band of solutions presented at the GAMM workshop.

Next, the alternate form of the axial momentum equation (12) is implemented in the shock region so that Euler solutions can be obtained. A comparison of a $M_\infty=0.8$ solution, with results given by Clarke et.al.[19] is shown in figure 4. The solutions are seen to be in good agreement with the present results, which predict a slightly sharper shock. Figure 5 presents a comparison of the present solution with the GAMM workshop results for a $M_\infty=0.85$ case. The band of solutions for the Euler case is seen to be much smaller than that for the full potential equation and again only the upper and lower bounds of solutions are presented. The present solution falls within this band and produces a sharper shock than those given in the workshop results.

In figure 6, the entropy generated along the airfoil for the $M_\infty=0.85$ case is compared with the value obtained from the Rankine-Hugoniot shock relations. The agreement is seen to be excellent. Two other important features should be noted. First, entropy is not generated ahead of the shock region. Secondly, the entropy generated at

the shock is convected properly downstream with no additional increase in entropy elsewhere.

The primary goal of this work, however, is to solve transonic, viscous interacting problems. The potential and Euler examples discussed herein have verified that the proper inviscid solutions are accurate, and therefore, should provide accurate outer flow behavior for full viscous calculations. The next set of results will describe solutions to the RNS equations for a variety of freestream Mach numbers and for a Reynolds number, $Re=4 \times 10^6$. Comparison of these solutions for an irrotational (potential) outer inviscid flow model and for a rotational (Euler) outer model flow is included in the discussion.

Results for $M_\infty=0.8$ are presented in figures 7a-c. In figure 7a the pressure coefficient is shown. Little difference is seen between the solutions with potential or Euler outer flows models. These results are also compared with experimental data [20]. The computed solution shows good agreement with the experimental results, except that the shock lies slightly aft of the experimental data. The skin friction coefficient for both outer flow conditions is compared in figure 7b. The effect of the outer flow is much more pronounced for the skin friction than was the case for the pressure coefficient. The skin friction has a much smaller decrease through the shock for the Euler outer flow. The oscillations in the skin friction coefficient at the leading edge are due to a lack of grid resolution and vanish at 10% of the chord. Finally, the Mach contours for $M_\infty=0.8$ are given in figure 7c.

Results for $M_\infty=0.83$ are presented in figures 8a-c. The pressure coefficient, figure 8a, is once again insensitive to the potential or Euler outer flow modeling, except in the post shock region where the

Euler outer flow provides a somewhat different character than that obtained with the potential outer flow. The computed results again show the shock located slightly aft of the experimental data. Also, the experimental results show a small increase in pressure ahead of the shock, which is not seen in the computed results. Only the Euler outer flow model provides the proper flow character after the shock. The reason for the difference in solutions after the shock can be seen from the skin friction results, figure 8b. The solution with a potential outer flow model has a small separated region after the shock. The solution with an Euler outer flow model does not separate and the skin friction is somewhat larger. Mach contours for the $M_\infty=0.83$ case are given in figure 8c.

The importance of the outer flow model becomes more apparent for the Mach number $M_\infty=0.85$. These results are given in figures 9a-c. The shock obtained with the potential outer flow model lies ahead of the shock obtained with the Euler outer flow model and again predicts a different post shock behavior. The skin friction coefficient figure 9b, shows that the Euler outer flow model leads to a rapid recovery after the shock with only a small separation region; the potential outer flow model produces a large region of separation. The rotationality in the outer flow appears to suppress the tendency toward separation. The Mach contour plot is given in figure 9c. Experimental results are not available for this case.

The potential, Euler, and RNS (Euler outer model) results for $M_\infty=0.8$ and $M_\infty=0.85$ are compared in figures 10 and 11, respectively. For $M_\infty=0.8$, the three solutions agree fairly well, with the Euler and RNS

solution being slightly weaker and lying forward of the potential shock. The rotational and viscous effects are of increased importance for the larger Mach number $M_\infty=0.85$. The Euler shock is weaker and lies forward of the potential shock. The RNS shock lies forward and is slightly weaker than the Euler shock. For the larger Mach numbers, shocks obtained from the full potential solution are too strong and are located far downstream of the RNS (Euler outer flow) results.

6. Summary

The composite velocity solution procedure has been applied for both viscous and inviscid transonic flows. Results are presented for flow over a NACA0012 airfoil. The results demonstrate the versatility of the composite velocity procedure. Both viscous and inviscid flows are solved from the same formulation with a simple change in the boundary conditions.

For inviscid flows, both irrotational potential solutions and rotational Euler solutions are obtained. For the Euler model, the axial momentum equation is given in a full conservation form in the shock region. This provides a solution technique that produces the correct entropy rise at the shock and at the same time convects the entropy accurately; no spurious entropy is created outside of shock regions. The potential and Euler solutions were found to agree with earlier results presented for the inviscid models.

Solutions for the RNS equations are obtained with potential and Euler outer models for a variety of Mach numbers. The results agree quite well with experimental results. The form of the outer flow model affects the post shock solution. Solutions with an irrotational outer flow tend to more readily induce post-shock separation, than do the

solutions with rotational outer flow modelling. The ability of the composite velocity procedure to efficiently calculate high Reynolds number transonic viscous flows attributes to the robustness of the solution technique.

Finally, the results for potential, Euler, and RNS (Euler outer modelling) solutions for several cases are compared. For higher Mach numbers, the Euler and potential solutions produce stronger shocks that are located further aft on the airfoil and do not accurately reflect the shock behavior.

7. Acknowledgement

This research was supported in part by the Air Force Office of Scientific Research under Contract F49620-85-C-0027 and in part under NASA Grant NAG I-8.

8. References

1. Khosla, P. K. and Rubin, S. G., "A Composite Velocity for the Compressible Navier-Stokes Equations," AIAA Journal, Vol. 21, No. 11, November, 1983, pp. 1546-1551.
2. Rubin, S. G. and Khosla, P. K., "A Composite Velocity Procedure for the Incompressible Navier-Stokes Equations," 8th International Conference on Numerical Methods in Fluid Mechanics, Springer-Verlag, 1982, pp. 448-454.
3. Swanson, R. C., Rubin, S. G., and Khosla, P. K., "Calculation of Afterbody Flows with a Composite Velocity Formulation," 16th Fluid and Plasma Dynamics Conference, July 12-14, 1983, AIAA Paper No. 834 1736.
4. Rubin, S. G., Celestina, M. and Khosla, P. K., "Second-Order Composite Velocity Solutions for Large Reynolds Number Flows," AIAA Paper No. 82-0099, AIAA 22nd Aerospace Sciences Meeting, Reno, Nevada, 1984.
5. Rubin, S. G. and Khosla, P. K., "Navier-Stokes Calculations with a Coupled Strongly Implicit Procedure," Computers and Fluids, Vol. 9, No. 2, 1979, pp. 163-180.
6. Cebeci, T., Smith, A. M. O., and Mosinski, G., "Calculations of Compressible Adiabatic Turbulent Boundary Layers," AIAA Journal, Vol. 8, No. 11, November, 1970, pp. 1974-1982.

7. Causon, D.M. and Ford, P.J., "Numerical Solutions of the Euler Equations Governing Axisymmetric and Three-Dimensional Transonic Flow," *Aeronautical Journal*, June/July, 1985.
8. Barton, J.T. and Pulliam, T.H., "Airfoil Computations at High Angles of Attack, Inviscid and Viscous Phenomena," *AIAA Journal*, Vol. 24, No. 5, May, 1986.
9. Osher, S. Hafez, M. and Whitlow, "Entropy Condition Satisfying Approximations for the Full Potential Equation of Transonic Flow," *Mathematics of computation*, Vol. 44, No. 169, January, 1985, pp. 1-29.
10. Davis, R. T., "Numerical Methods for Coordinate Generation Based on Schwarz-Christoffel Transformations," *AIAA Paper No. 79-1463*, *AIAA Computational Fluid Dynamics Conference*, Williamsburg, Virginia, 1979.
11. Rizzi, A. and Viviani, H.(Eds.), "Numerical Methods for the Computation of Inviscid Transonic Flows with Shock Waves: A GAMM Workshop," *Friedr.Vieweg & Sohn*, 1981.
12. Schmidt, W. "Recent Developments in Finite-Volume Time Dependent Techniques for Two and Three Dimensional Transonic Flows," *Lecture Notes for Series on Computational Fluid Dynamics*, Von Karman Institute for Fluid Dynamics, March 29 - April 2, 1982.
13. Baker, T. J., "The Computation of Transonic Potential Flow," *Lecture Notes for Series on Computational Fluid Dynamics*, Von Karman Institute for Fluid Dynamics, Brussels, Belgium, March 30 - April 3, 1981.
14. Chow, L. J., Pulliam, T. H., and Steger, J. L., "A General Perturbation Approach for the Equations of Fluid Dynamics," *AIAA Paper No. 83-1903*, *AIAA Computational Fluid Dynamics Conference*, Danvers, Massachusetts, 1983.
15. South, J.C., Keller, J. D., and Hafez, M., "Vector Processor Algorithms for Transonic Flow Calculations," *AIAA Paper No.79-1457*, *AIAA Computational Fluid Dynamics Conference*, Williamsburg, Virginia, 1979.
16. Hafez, M. and Lovell, D., "Numerical Solution of Transonic Stream Function Equation," *AIAA Paper No. 81-1017*, *AIAA Computational Fluid Dynamics Conference*, Palo Alto, California, 1981.
17. Sherif, A. and Hafez, M., "Computation of Three Dimensional Transonic Flows Using Two Stream Functions," *AIAA Paper No. 83-1948*, *AIAA Computational Fluid Dynamics Conference*, Danvers, Massachusetts, 1983.
18. Wong Y. S. and Hafez, M., "Application of Conjugate Gradient Methods to Transonic Finite Difference and Finite Element Methods," *AIAA Paper No. 81-1032*, *AIAA Computational Fluid Dynamics Conference*, Palo Alto, California, 1981.

19. Clarke, D.K., Salas, M.D., and Hassan, H.A., "Euler Calculations for Multi-element Airfoils Using Cartesian Grids," AIAA Journal, Vol. 24, No. 3, March, 1986.
20. "Experimental Data Base for Computer Program Assessment," AGARD Advisory Report No. 138.
21. Pandolfi, M., "The Merging of Two Different Ideas: A Shock Fitting Performed by a Shock Capturing," International Symposium on Computational Fluid Dynamics Tokyo, September 9-12, 1985.

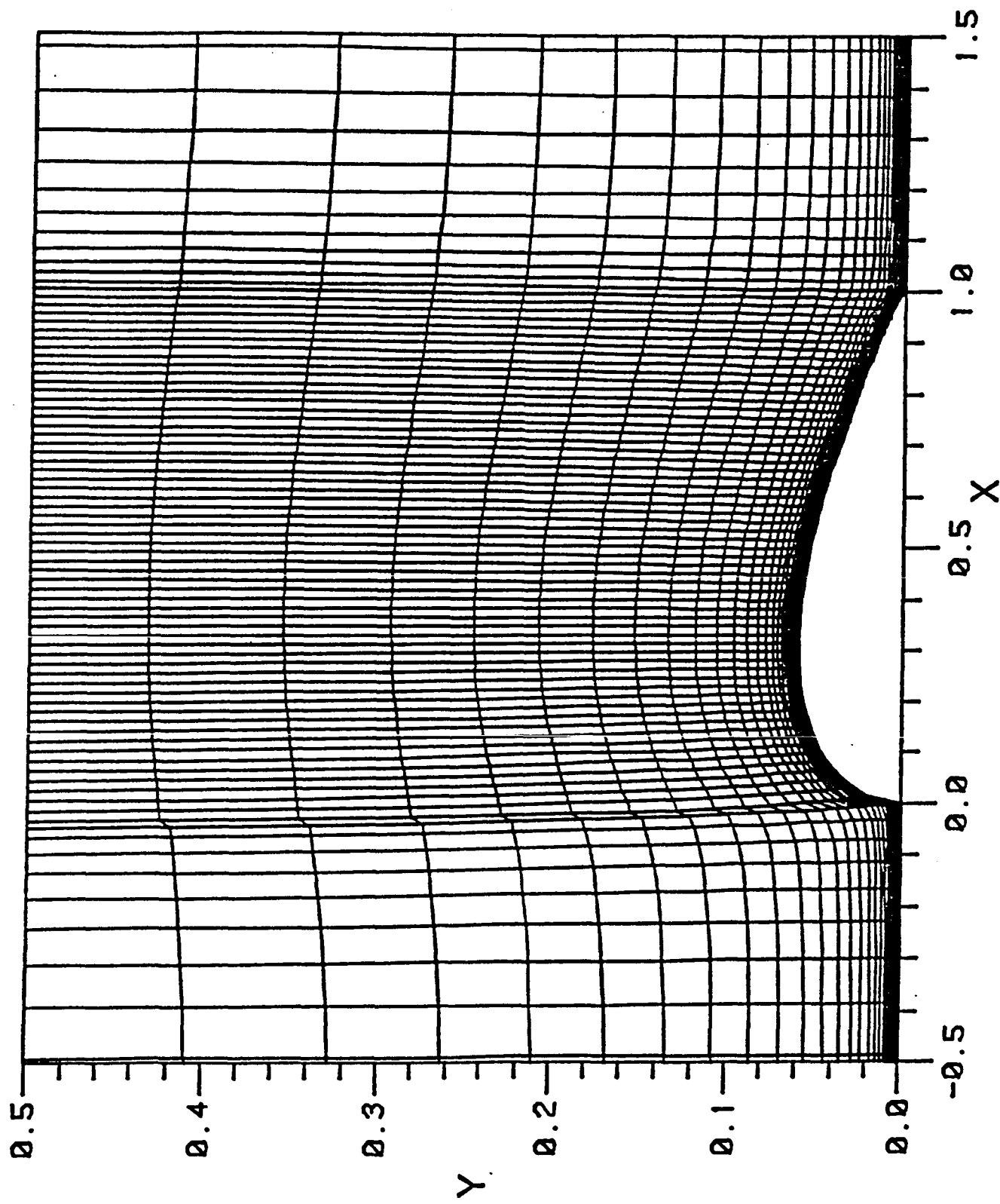


Figure 1. Viscous Grid for an NACA0012 Airfoil

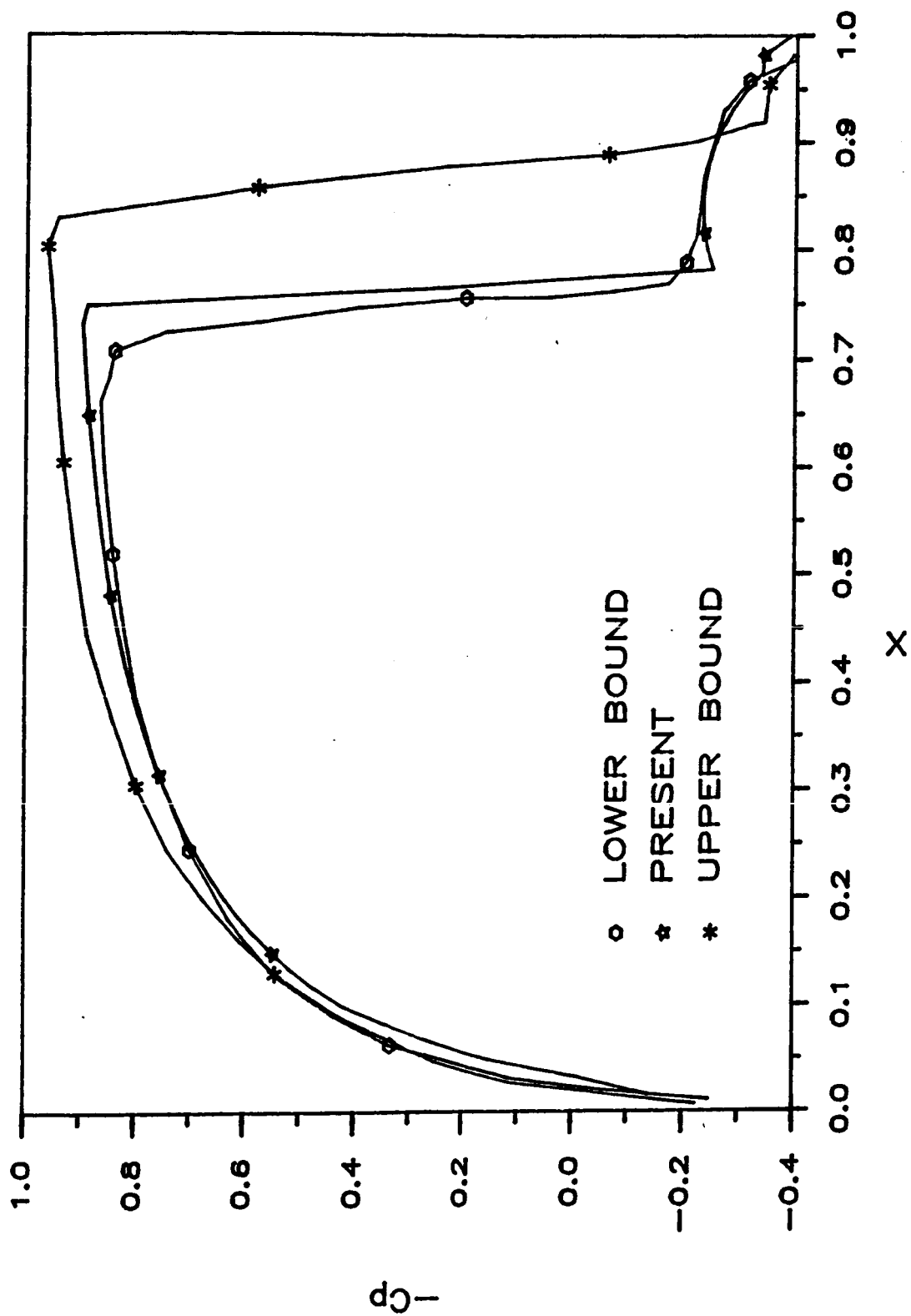


Figure 2. Comparison of Potential Solution for an
NACA0012 Airfoil, $M_\infty = 0.85$

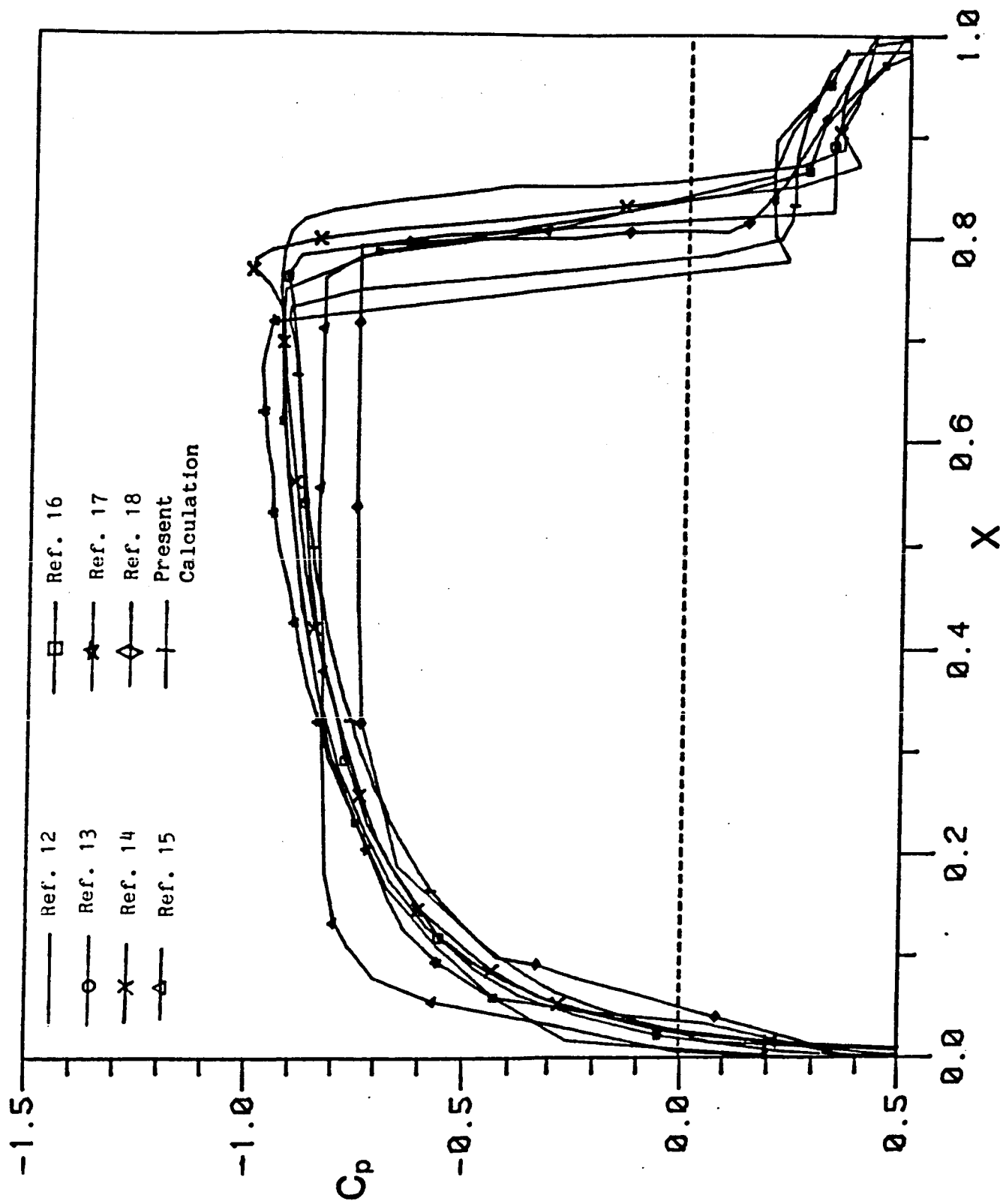


Figure 3. Comparison of Present Potential Solution with Various other Potential Solutions for an NACA0012 Airfoil

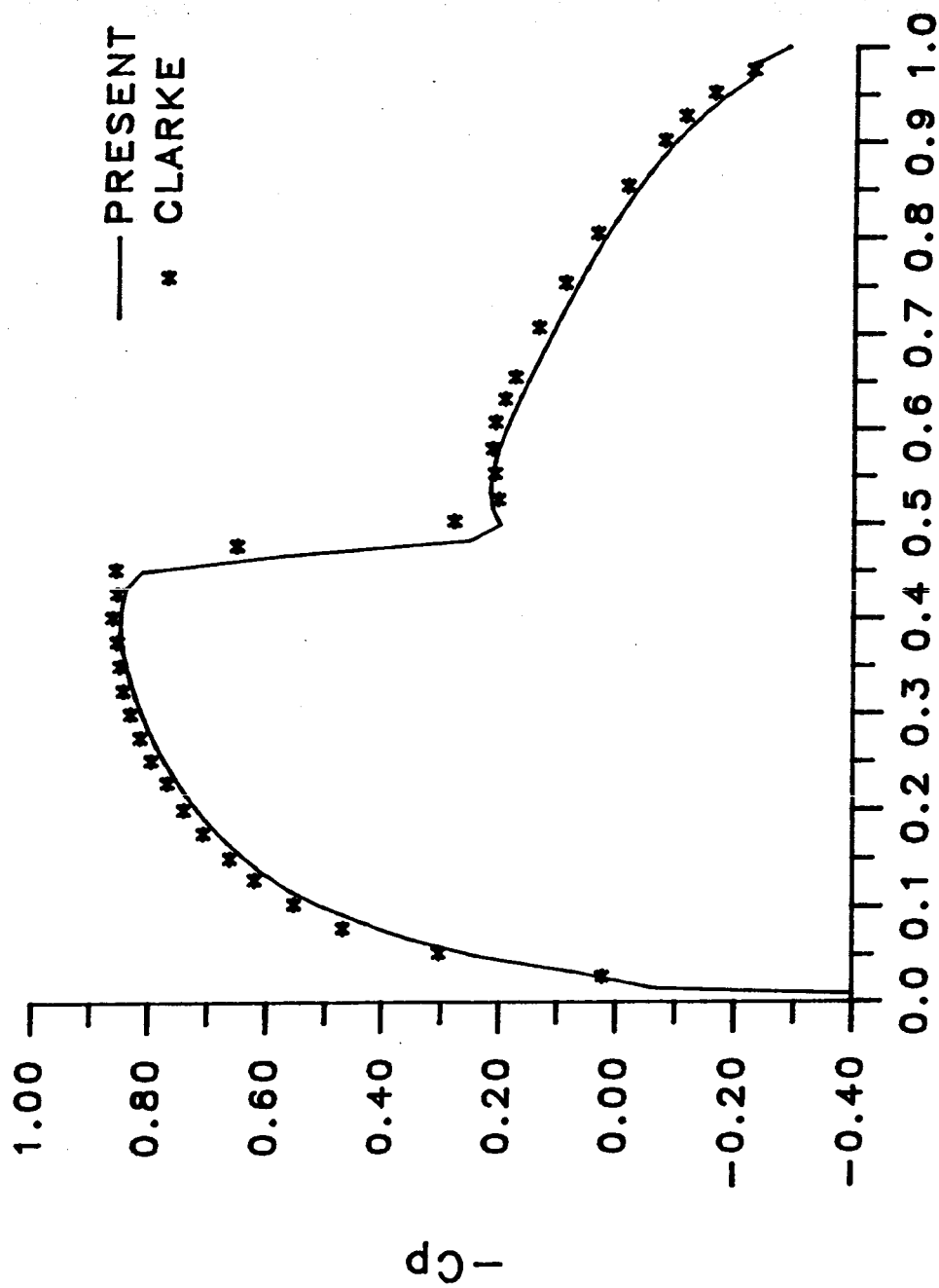


Figure 4. Comparison of Euler Solution
for an NACA0012 Airfoil, $M_\infty = 0.8$

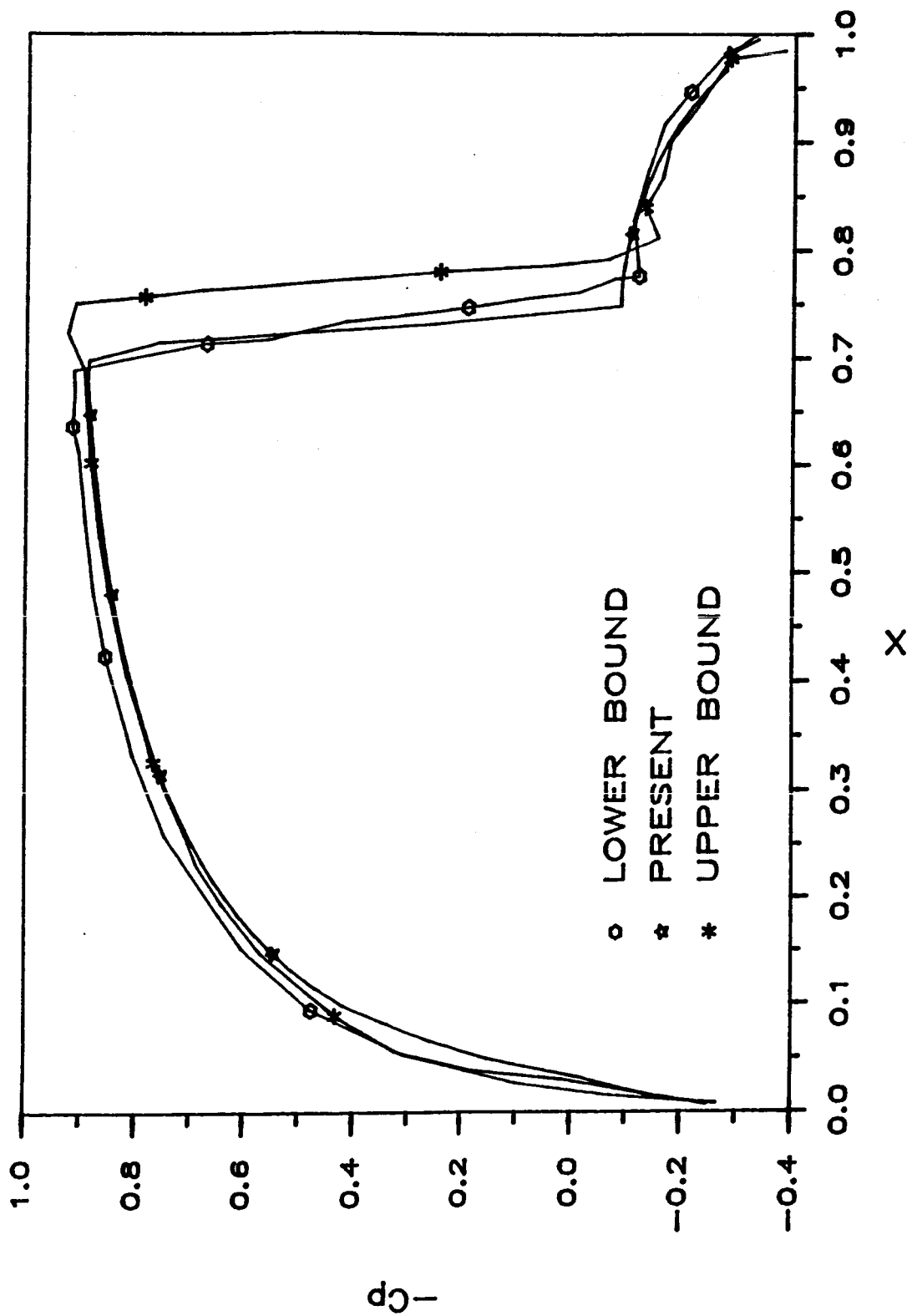


Figure 5. Comparison of Euler Solution for an NACA0012 Airfoil, $M_\infty = 0.85$

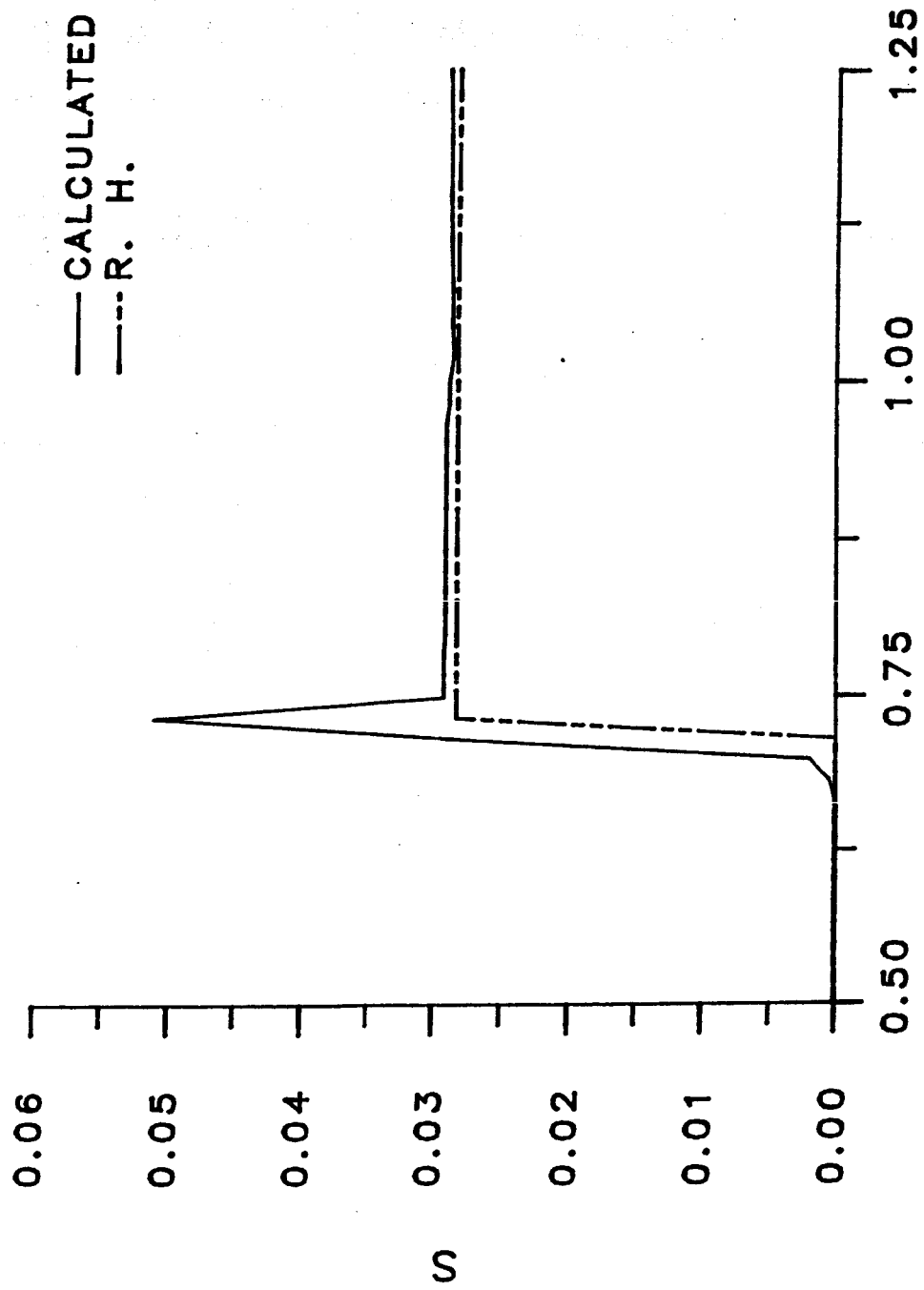


Figure 6. Comparison of Entropy along an NACA0012 Airfoil with the Rankine-Hugoniot Value, $M_\infty = 0.85$

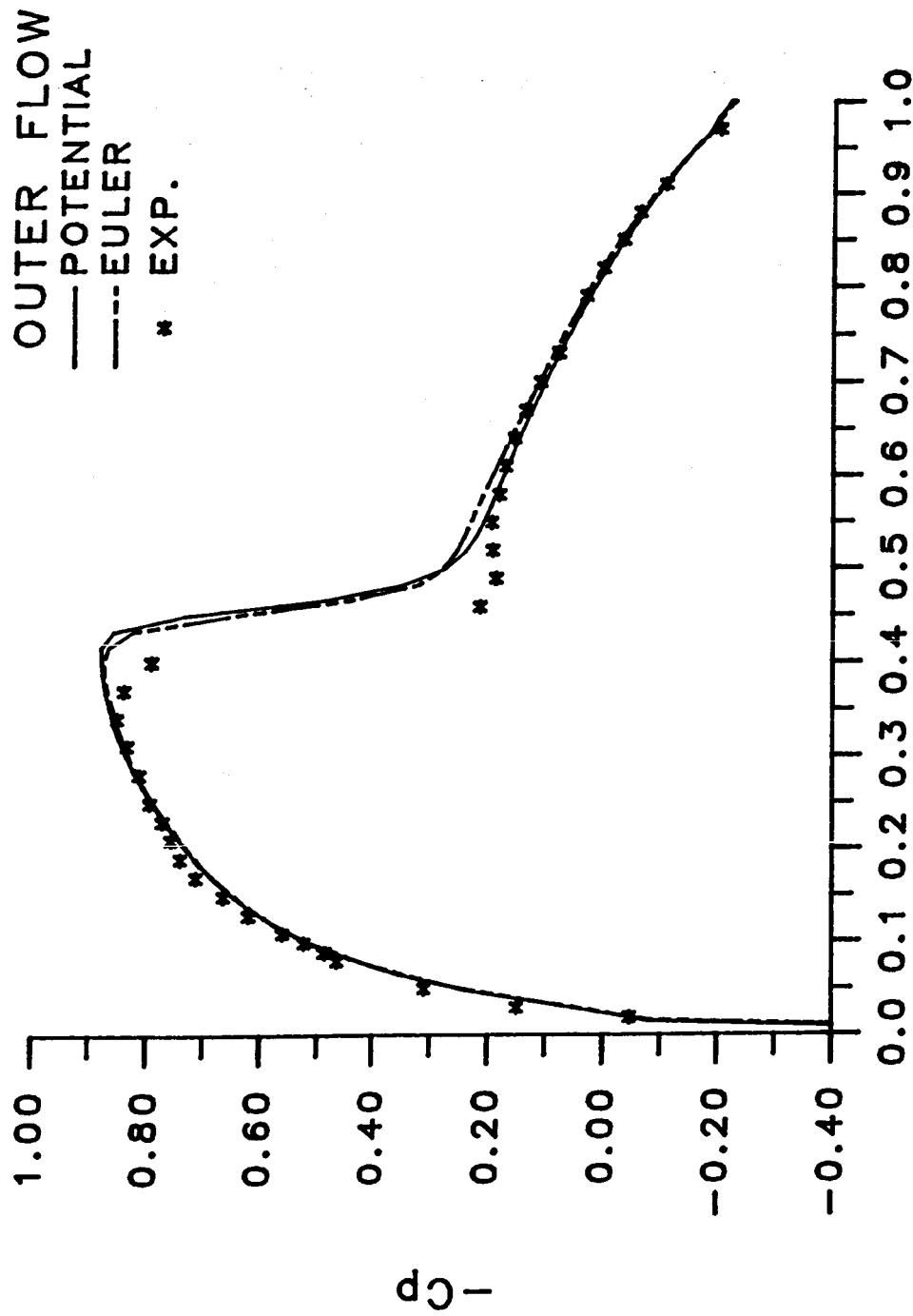


Figure 7a. R.N.S. Solution for an NACA0012
 Airfoil, $M_\infty = 0.8$, $Re = 4.0 \times 10^6$;
 Comparison with Different Outer Flows

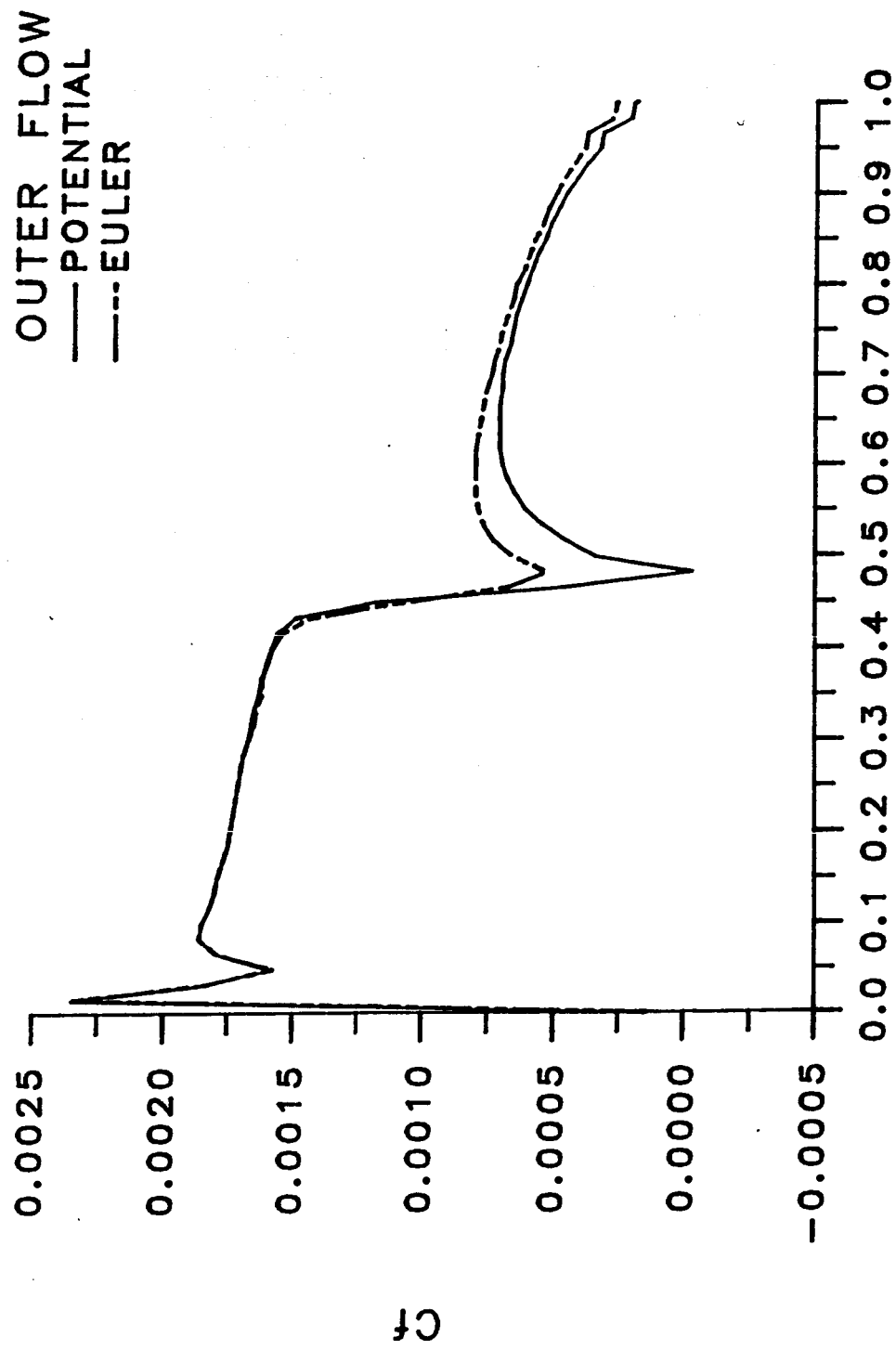


Figure 7b. R.N.S. Solution for an NACA0012
 Airfoil, $M_\infty = 0.8$, $Re = 4.0 \times 10^6$;
 Comparison with Different Outer Flows

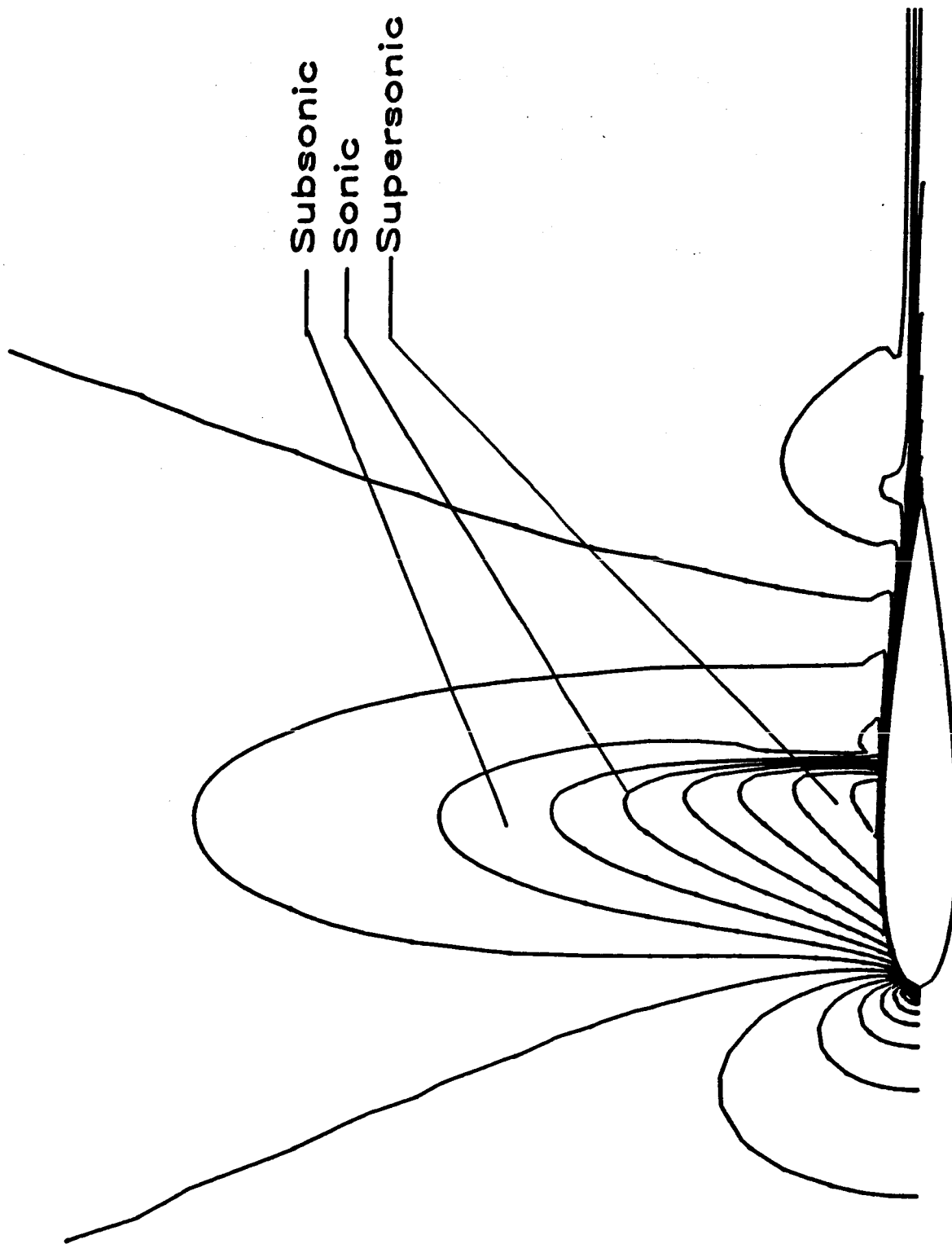


Figure 7c. Mach Contours for an NACA0012
Airfoil, $M_{\infty}=0.8$, $Re=4.0 \times 10^6$;
R.N.S. Solution with Euler Outer Flow

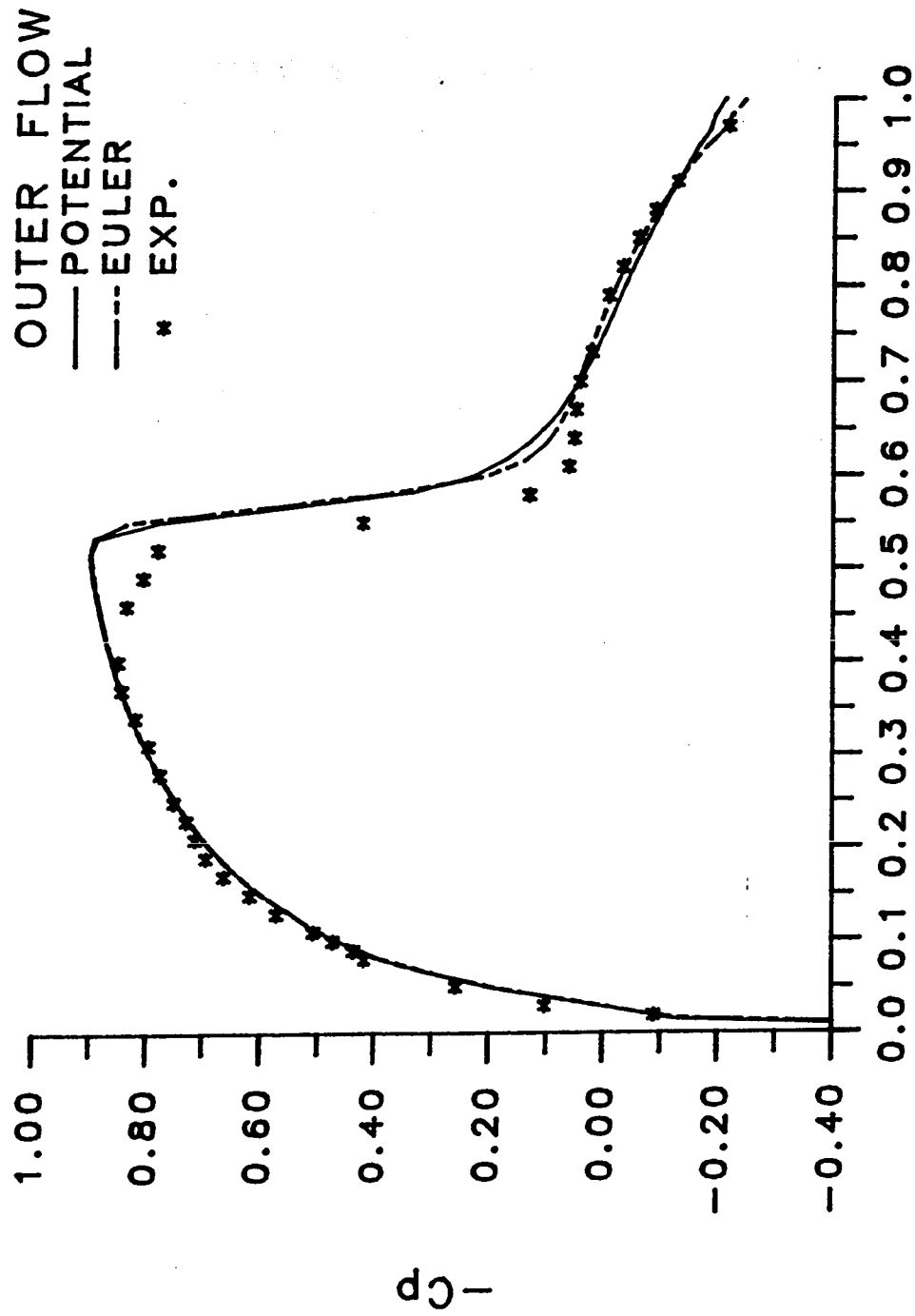


Figure 8a. R.N.S. Solution for an NACA0012
 Airfoil, $M_\infty=0.83$, $Re=4.0 \times 10^6$;
 Comparison with Different Outer Flows

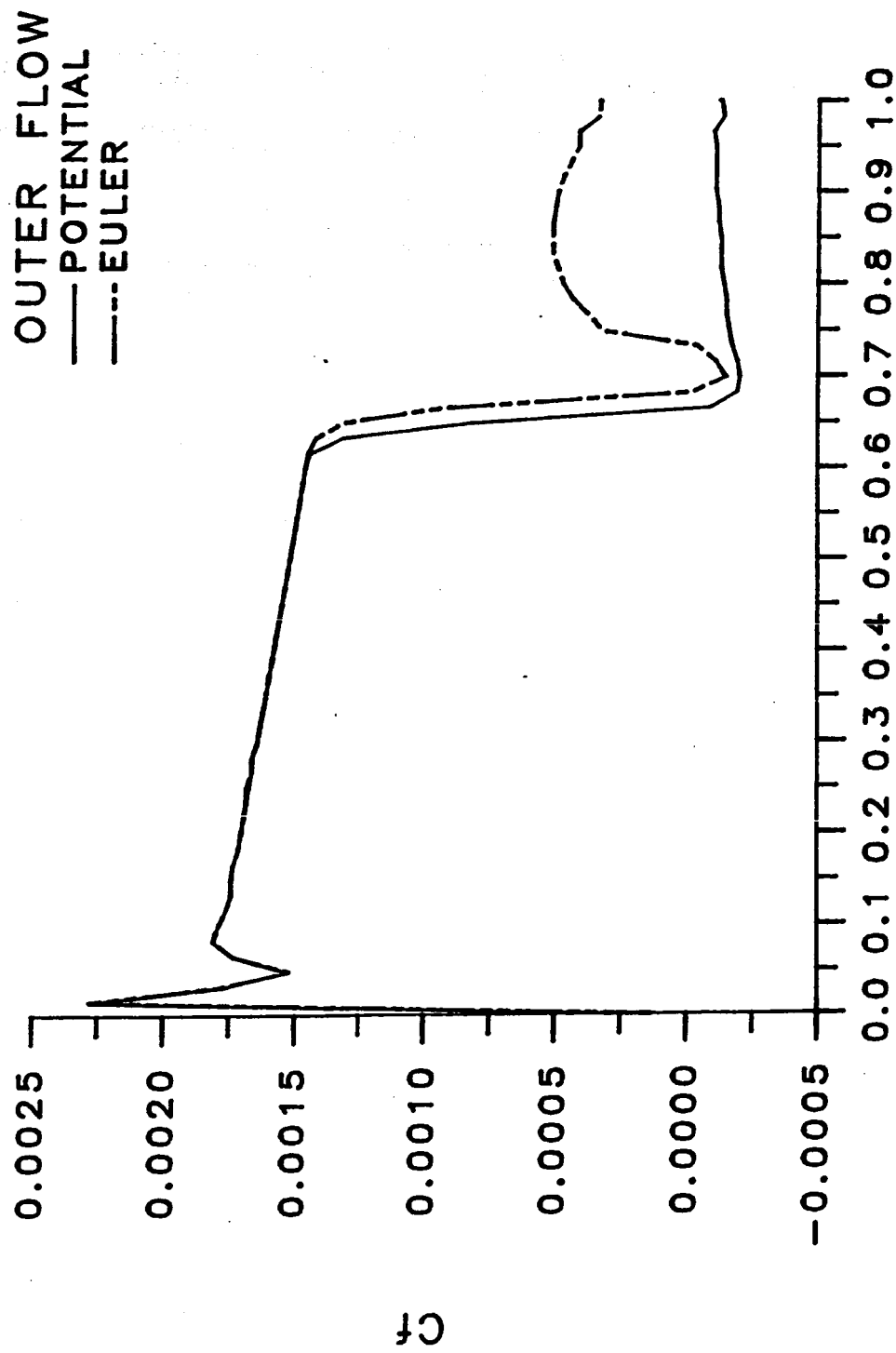


Figure 9b. R.N.S. Solution for an NACA0012 Airfoil, $M_\infty=0.85$, $Re=4.0 \times 10^6$; Comparison with Different Outer Flows

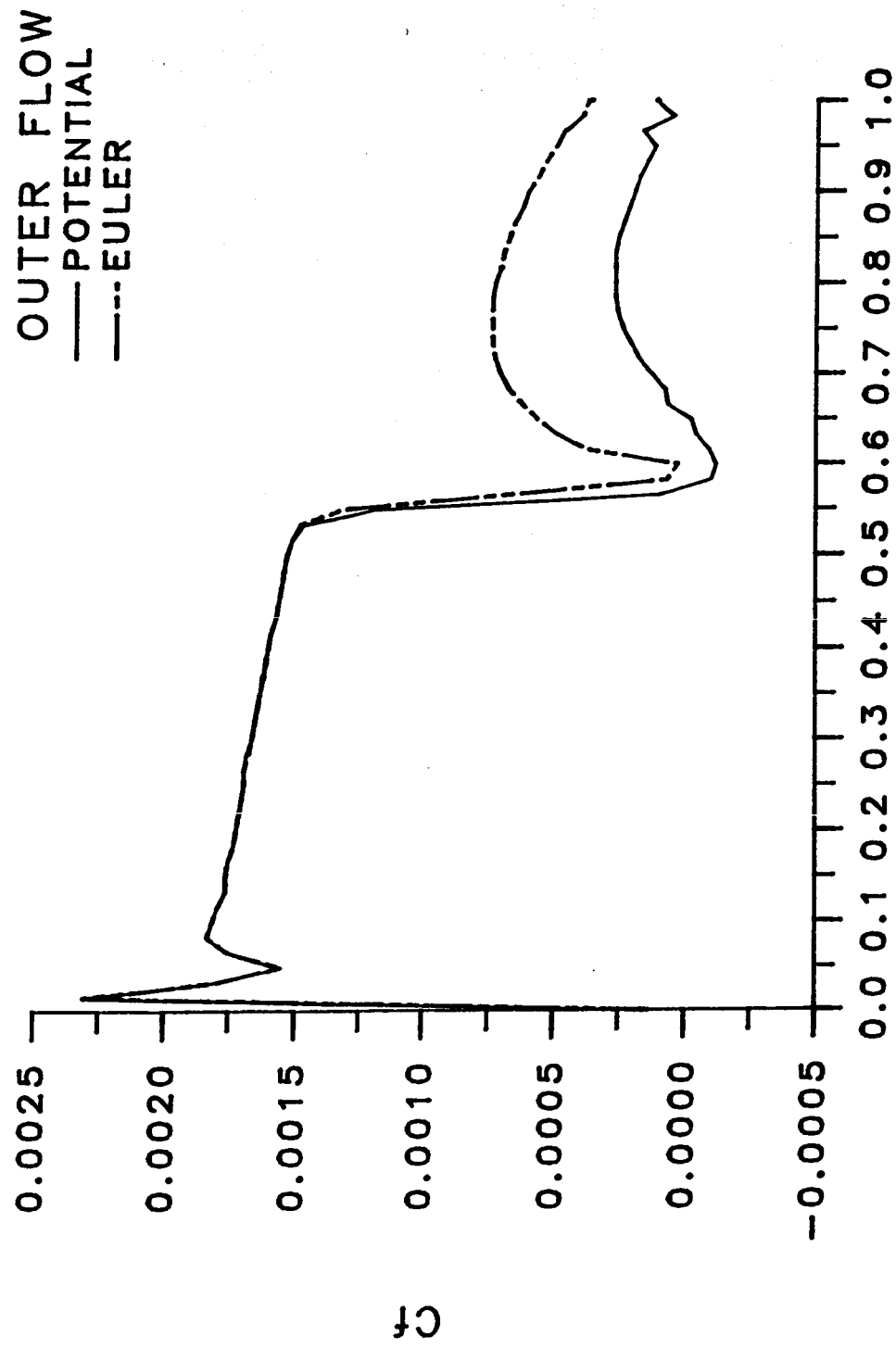


Figure 8b. R.N.S. Solution for an NACA0012 Airfoil, $M_\infty=0.83$, $Re=4.0 \times 10^6$; Comparison with Different Outer Flows

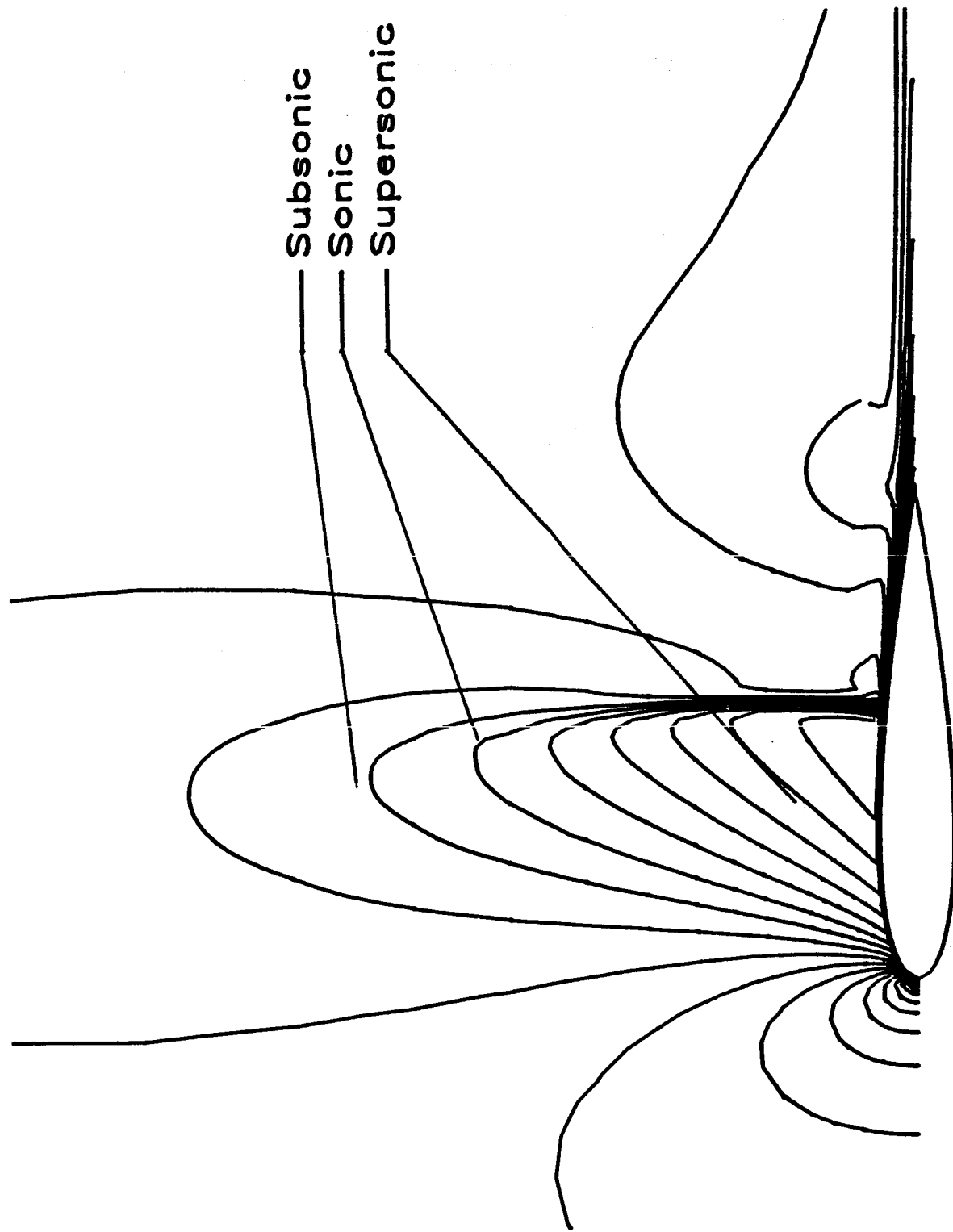


Figure 8c. Mach Contours for an NACA0012
Airfoil, $M_\infty=0.83$, $Re=4.0 \times 10^6$;
R.N.S. Solution with Euler Outer Flow

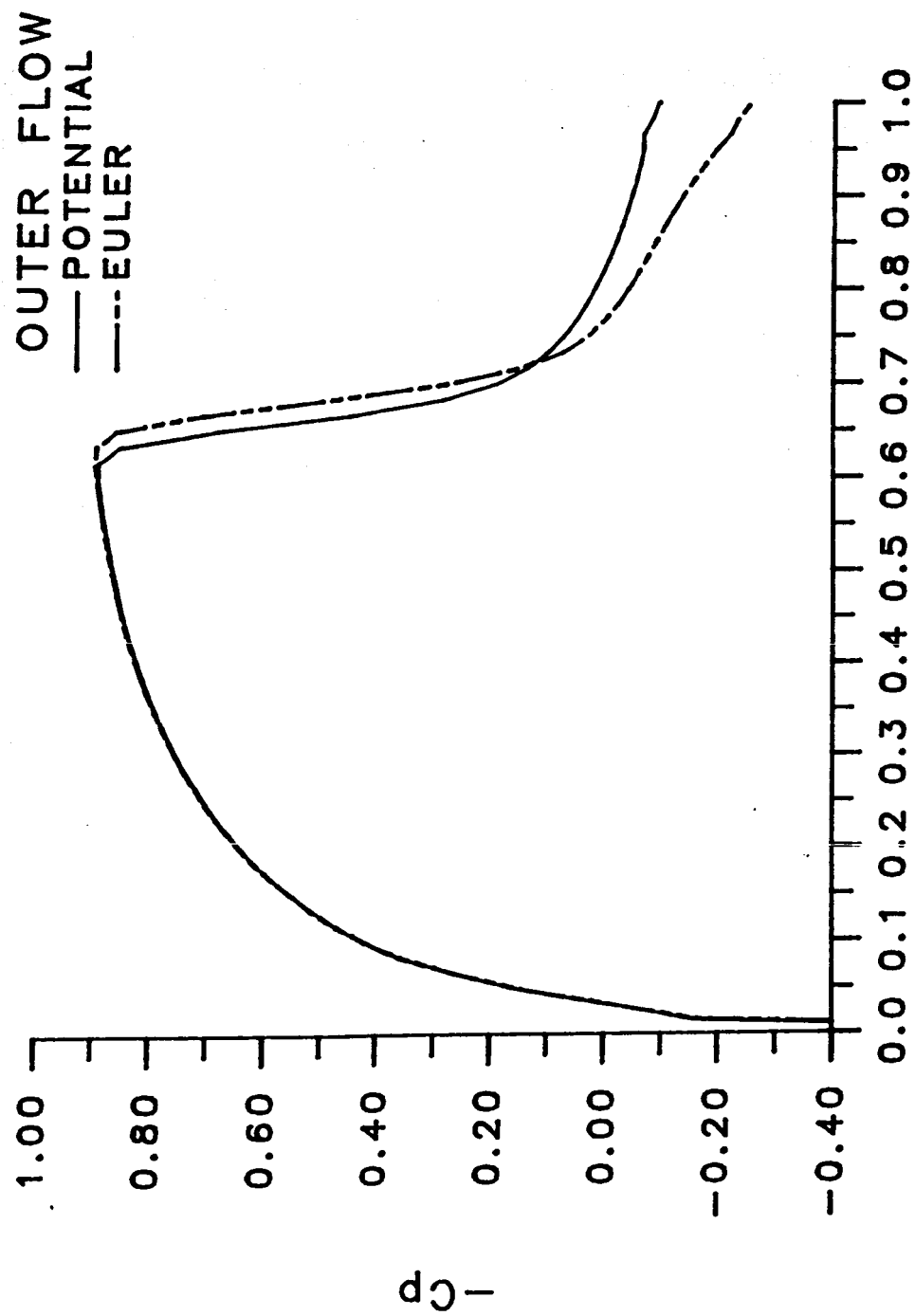


Figure 9a. R.N.S. Solution for an NACA0012 Airfoil, $M_\infty=0.85$, $Re=4.0 \times 10^6$; Comparison with Different Outer Flows

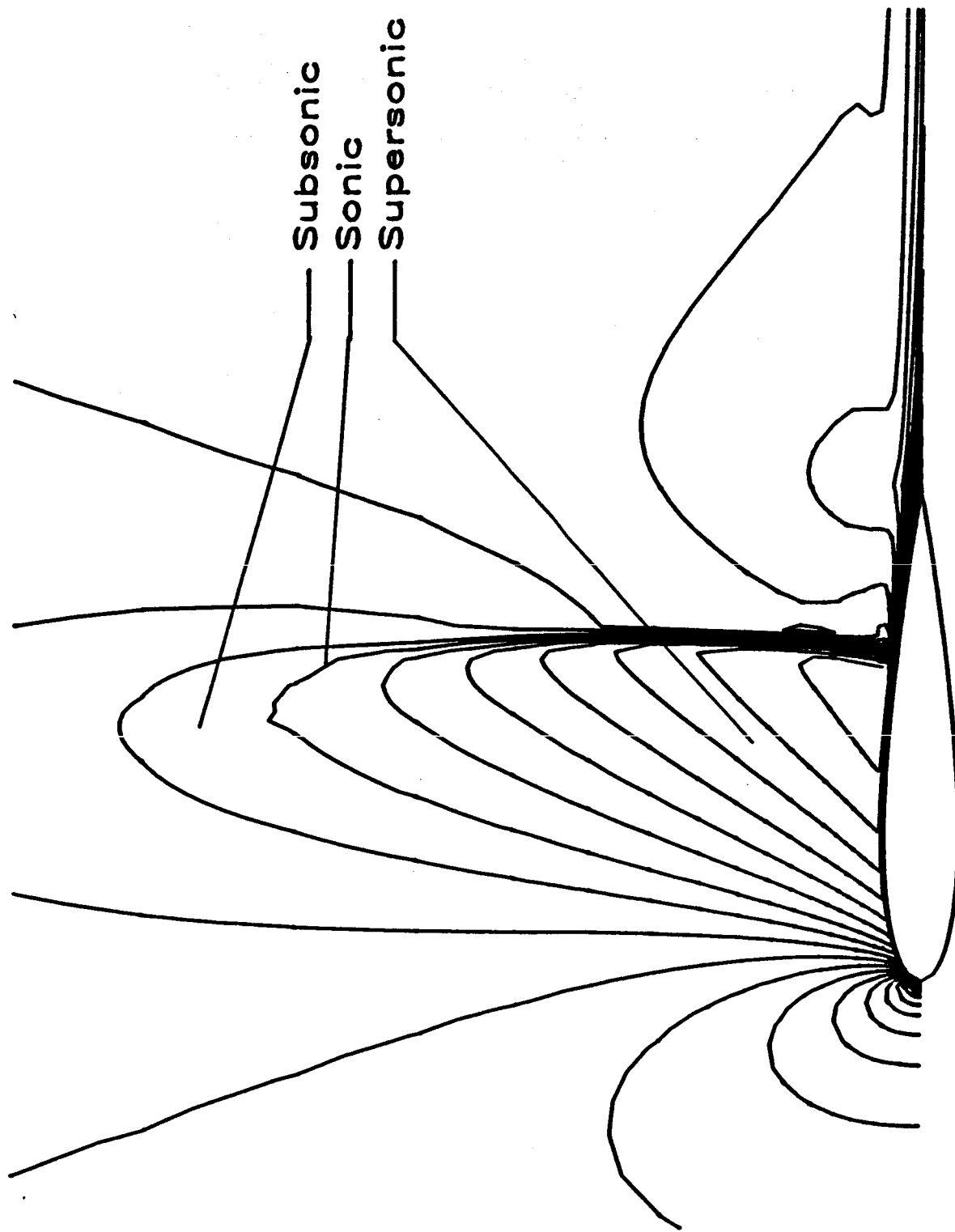


Figure 9c. Mach Contours for an NACA0012 Airfoil, $M_\infty=0.85$, $Re=4.0 \times 10^6$; R.N.S. Solution with Euler Outer Flow

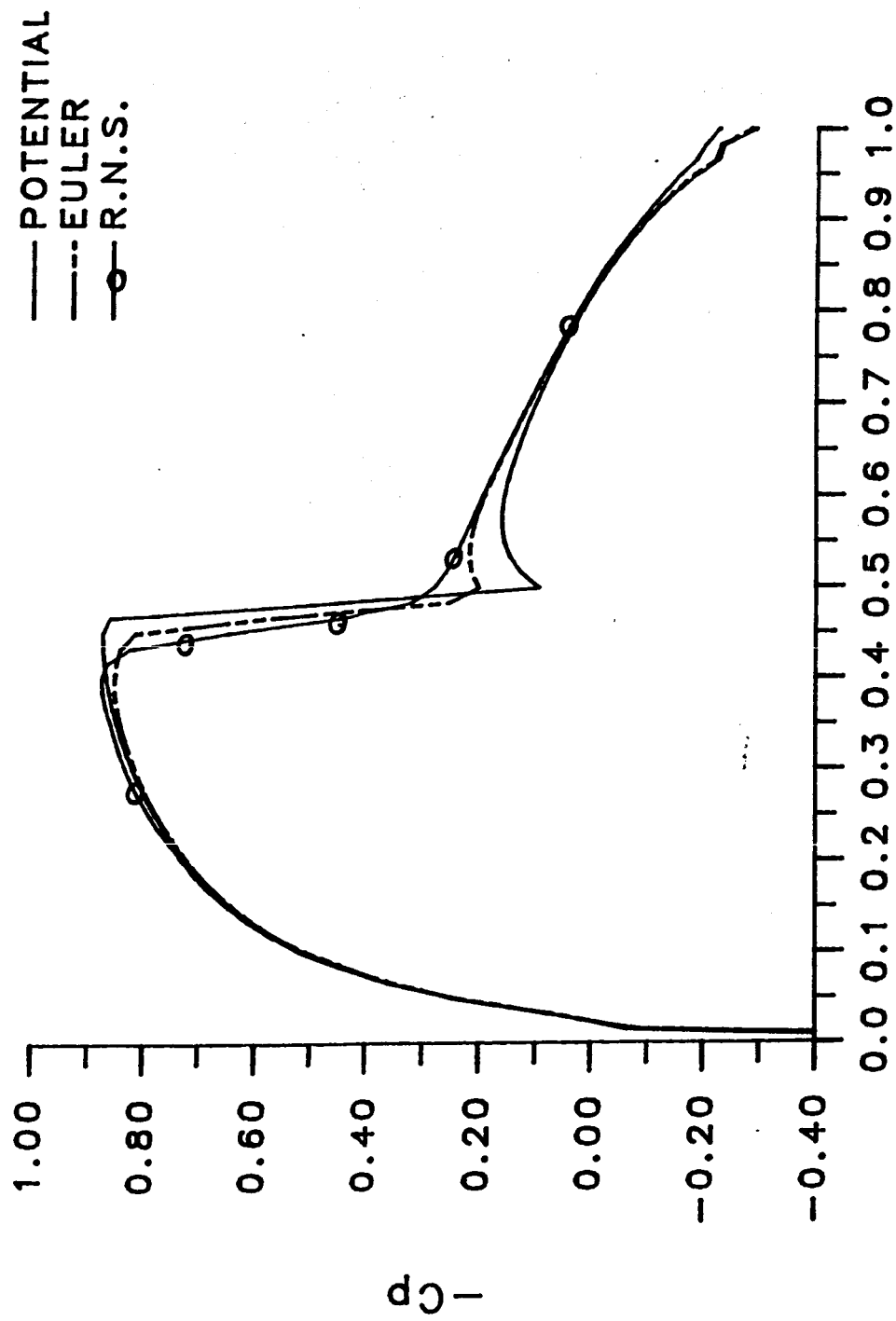


Figure 10. Comparison of Solutions for an
NACA0012 Airfoil, $M_\infty=0.8$;
Composite Velocity Formulations

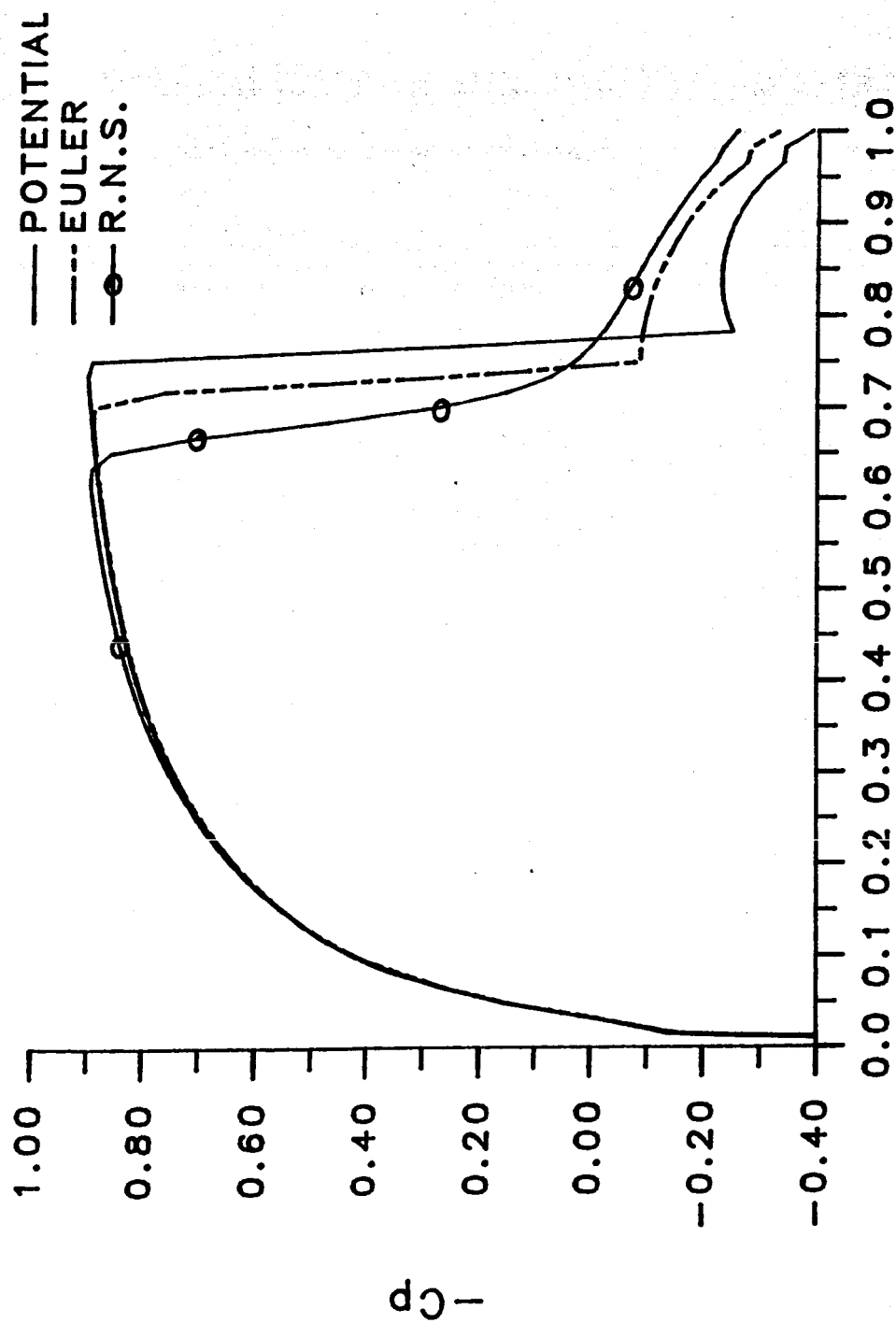


Figure 11. Comparison of Solutions for an
NACA0012 Airfoil, $M_{\infty}=0.85$;
Composite Velocity Formulations